6. Other Research Activities

Inside:

- Penta-graphene Nanocone
- Buckling Load Estimation for Double-walled Carbon Nanotube
- Critical Evaluation of Fractional calculus based on Eringen's nonlocal model for 1-D wave propagation
- The Warming Mode of Tropical Indian Ocean Surface
- A Seasonal Cycle relevant to El Nino-Southern Oscillation

6.1 Penta-graphene Nanocone

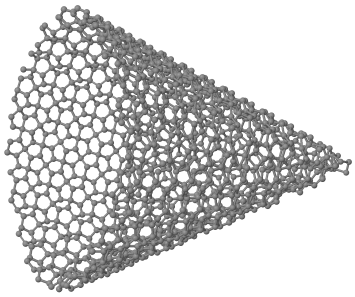

Figure 6.1: Penta-graphene nanocone.

The present work aims to generate the coordinates for the penta-graphene nanocone (Figure 6.1) structure. The main difference between carbon nanocone and penta-graphene is the number of atoms. The penta-graphene structure consists of five carbon atoms, while carbon nanocone consists of six carbon atoms. In the literature, there exists no attempt to explore such a structure. The indigenous software code helps in generating the coordinates. The penta-graphene nanocone structure development is tricky because of penta-graphene atoms located in different planes. The mechanical properties of this structure are of greater interest to researchers in further applications in nanotechnology areas.

6.2 Buckling Load Estimation for Double-walled Carbon Nanotube

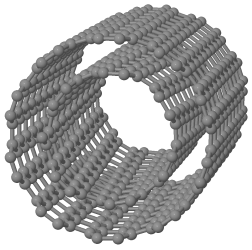

Figure 6.2: Double-walled carbon nanotube.

The Euler critical buckling loads of double-walled carbon nanotube (Figure 6.2) are estimated using a semi-analytical method. Many approximate numerical methods determined the critical buckling loads in the literature. But the present study corrects the typographical mistakes in the previous literature study. Unlike different numerical methods that estimate the buckling loads for various boundary conditions, the semi-analytical method predicts robust results, which works well for any boundary conditions. The five different boundary conditions used in the present investigation are simply-simply, clamped-clamped, clamped-simply, clamped-free, and clamped-sliding restraint. Also, unlike other methods, the present methodology is free from polynomial development.

6.3 Critical Evaluation of Fractional calculus based on Eringen's nonlocal model for 1-D wave propagation

In recent years, fractional calculus attracted researchers in modeling nanostructure with nonlocal continuum elasticity. The wave propagation study reveals that the nonlocal fractional model based on Eringen's model predicts the dispersion curve with an excellent match compared to lattice dynamics. Even the phase velocity results gave fantastic results with lattice dynamics. But the group velocity results show that it fails to match with lattice dynamics results at the end of the first Brillouin zone. So this compromise has to be made if a nonlocal fractional calculus model based on Eringen's model is used for the wave propagation approach.

6.4 The Warming Mode of Tropical Indian Ocean Surface

The Sea Surface Temperature (SST) in the tropical Indian Ocean (IO) has monotonically warmed about one-degree centigrade since 1950; this has been attributed to the increasing greenhouse gas in the atmosphere. The remotely induced changes in local wind, ocean circulation, and surface-flux also modify IO SST variability on interannual time scales. Both change local deep atmospheric convection patterns and alter the climate phenomena like Asian Monsoons and El Nino Southern Oscillation. Spatial patterns of remotely-forced responses may be different from those generated by anthropogenic factors. Therefore, their influences on weather and climate events also differ. Moreover, the Spatio-temporal characteristics of the observed warming of the IO SST and its statistical link to the Indian Ocean Warm Pool (IOWP) are still unclear. The observed patterns and rates of warming estimated via linear regression are sensitive to duration and epoch under consideration. The linear methods also fail to differentiate the spatial patterns of SST associated with the multi-decadal warming from those remotely forced. However, the discrimination of their response patterns is necessary for future climate prediction and climate change adaptation. This study discriminates the basin-wide monotonic warming mode of the IO surface from the internally and remotely forced variability. Instead of the amorphous trend patterns reported earlier, the radically different warming signal reported shows that the monotonic warming in the observed IO SST has the spatial pattern of summer-mean SST and the Warm Pool as its most conspicuous feature. The highest warming is (0.17 ^{0}C per decade) in the IOWP and not in the other IO regions identified in the previous studies. By 2070, the IOWP will cover about 80 percent of tropical IO at the present latitudinal expansion rates. The mean states of SST, wind, and surface pressure are shifting towards an endless summer. Irrespective of the season, the SST near Indonesia would likely remain above 31 ^{0}C by 2080 and beyond; this would substantially increase local rainfall intensity and frequency. We also argue that the basin-wide warming is due to anthropogenic forces' rectification by coupled processes in ocean-atmosphere mixed layers.

6.5 A Seasonal Cycle relevant to El Nino-Southern Oscillation

The most remarkable features captured by climate modes of five variables in the Pacific are the sub-seasonal developments of cold/warm SST in equatorial EP, and positive/negative OLR extending from WP to EP along the Equator; they pattern-wise resemble those associated with the canonical La Nina/El Nino. The positive (negative) SST anomalies appear in March (September), peak in May (December), and decay by August (February). From March to July, nearly the whole tropical pacific is covered by a cyclonic wind system and the opposite one from September to December. These wind systems emanate from the band of subtropical high-SLP and culminate in the band of low-SLP in the opposite hemisphere. The equatorial waveguide during these two periods is occupied by a reversing wind system. During the warm SST phase (i.e., March to July), the north-easterly wind (predominated by northerly component over the north of the Equator) becomes north-westerly

as it crosses the Equator. This wind system increases SST by suppressing upwelling along the Equator and the eastern coastlines, causing a subsequent reduction in latent heat loss and further enhancement of magnitude and westward expansion of SST along the Equator. The intensification of both the wind converges and negative OLR over the equatorial region occurs. The cold SST phase (i.e., September to January) is driven by a nearly opposite wind system and suppressed convection; both of which are initiated around September. Such wind system generates cold water upwelling to further lower SST and suppress the convection. Similar observed relationships between SST, wind, SLP, low-level wind convergence, and atmospheric convection have been evoked often to explain many elements of tropical variability. It is instructive to note that the intensification of positive (negative) SST after March (October) are, not by coincidence, also the onset months of ENSO anomaly.